La0.7Sr0.3MnO3 thin films on SrTiO3 and CaTiO3 buffered Si substrates: structural, static, and dynamic magnetic properties

Mohamed Belmeguenai, Sylvana Mercone, Carlo Adamo, T. Chauveau, Laurence Méchin, P. Monod, D.G. Schlom

$La_{0.7}Sr_{0.3}MnO_3$ thin films on $SrTiO_3$ and $CaTiO_3$ buffered Si substrates: structural, static, and dynamic magnetic properties

M. Belmeguenai · S. Mercone · C. Adamo · T. Chauveau · L. Méchin · P. Monod · P. Moch · D. G. Schlom

Abstract Nearly 50-nm thick $La_{0.7}Sr_{0.3}MnO_3$ (LSMO) films were grown on Si substrates using molecular beam epitaxy on (001) Si substrates overlayered by a 20 nm thick $SrTiO_3$ (STO) or by a 20 nm thick $CaTiO_3$ (CTO) film. In addition, a reference LSMO film was directly deposited on a (001) STO substrate by pulsed laser deposition. For all the samples, X-ray diffraction revealed an excellent epitaxy of the LSMO film and small mosaicity around (001), with in-plane [100] and [010] cubic axes. The LSMO/CTO films are in-plane compressed while the LSMO/STO ones are in-plane extended. The temperature dependence of their static magnetic properties was studied using a SQUID, showing a Curie temperature overpassing 315 K for all the samples. Hysteresis loops performed at room temperature (294 K) with the help of a vibrating sample magnetometer (VSM) are also discussed. At 294 K Micro-strip ferromagnetic resonance (MS-FMR) was used to investigate the dynamic magnetic properties. It allows concluding to a strong anisotropy perpendicular to the films and to a weak fourfold in-plane anisotropy with easy axes along the [110] and [1$\bar{1}$0] directions. Their values strongly depend on the studied sample and are presumably related to the strains suffered by the films.

Keywords Magnetic manganites · Magnetic anisotropy · Ferromagnetic resonance · Nanocomposites

M. Belmeguenai (✉) · S. Mercone · T. Chauveau · P. Moch
LSPM (UPR 3407) CNRS, Université Paris-13, Avenue J.-B. Clément, 93430 Villetaneuse, France
e-mail: belmeguenai.mohamed@univ-paris13.fr

C. Adamo · D. G. Schlom
Department of Materials Science and Engineering, Cornell University, Ithaca, NY 14853-1501, USA

L. Méchin
GREYC (UMR 6072) CNRS, ENSICAEN, Université de Caen Basse-Normandie, 6 Boulevard Maréchal Juin, 14050 Caen Cedex, France

P. Monod
LPEM (UPR A0005) CNRS, ESPCI, 10 Rue Vauquelin, 75231 Paris Cedex 5, France

Introduction

Spintronics, introduced more than 15 years ago, revives the interest in the perovskite manganites, generally referred to as colossal magnetoresistance (CMR) materials. $La_{0.7}Sr_{0.3}MnO_3$ (LSMO), which belongs to this family, is expected to have a spin polarization close to 100% (half metal) (Bowen et al. 2003) and, therefore, can be used in a number of spin-dependent transport devices grown on insulating matching substrates ($SrTiO_3$ and $NdGaO_3$), such as magnetic tunneling junctions (Bowen et al. 2003; Ishii et al. 2005) and spin valves (Xiong et al. 2004; Dediu et al. 2002). Moreover, LSMO is a good

candidate for spin injection into semiconductors, due to its low carrier density, the high spin polarization of its charge carriers and to its ferromagnetism up to above room temperature (Park et al. 1998). Therefore, the integration of LSMO as source of spin polarized carriers in semiconductor based devices is a challenging task for potential applications that utilize both information processing and data storage in the same device, such as high-density magnetic memories and magnetic sensors.

Since the development of hybrid LSMO–Si based spintronic devices requires good control of their magnetic properties, the aim of this paper is to investigate the static as well as dynamic magnetic properties of LSMO thin films deposited on a Si substrate preliminary overlaid with a thin $SrTiO_3$ (STO) or $CaTiO_3$ (CTO) buffer layer. The temperature dependence of their static magnetic properties is studied using a SQUID. Micro-strip line ferromagnetic resonance (MS-FMR) is used for a full magnetic dynamic characterization at room temperature.

In "Samples and experimental setups" section, we describe the samples, their preparation, and their structural characterization. "Results and discussion" section presents the experimental results and the magnetic parameters derived from our data using a simple model which is briefly exposed. Conclusions are presented in final section.

Samples and experimental setups

We have prepared $La_{0.7}Sr_{0.3}MnO_3$ films overlaying 20-nm thick $SrTiO_3$ (STO) or $CaTiO_3$ (CTO) templates that we grew on Si (001) substrates by a reactive molecular beam epitaxy (MBE) system. The substrate temperature was fixed at 670 °C and an ozone background pressure of 3×10^{-7} Torr was used. The single elements strontium, manganese, and lanthanum were evaporated from effusion cells. The detailed description of the STO and CTO template layers preparation procedure is presented in Warusawithana et al. (2009). In addition, for comparison, a reference LSMO layer was grown by pulsed laser deposition on a STO (001) substrate. In all the samples the LSMO thickness is approximately equal to 50 nm. For the LSMO/STO/Si and LSMO/STO systems, it was precisely measured using X-rays or neutron reflectivity, providing 58 and 51 nm, respectively. In addition, we proceeded to X-ray diffraction study consisting in θ–2θ recordings, followed by ω rocking measurements and pole figure investigations: it results that the LSMO films are fully

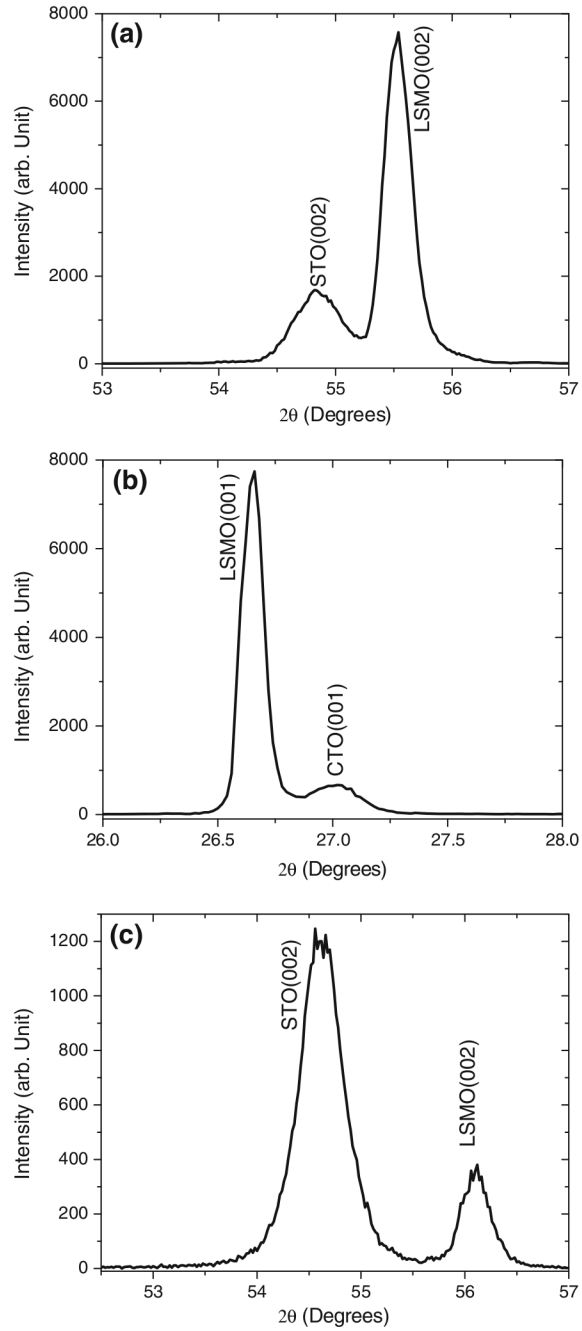

Fig. 1 X-rays Bragg scan using the Co Kα radiation for the a LSMO/STO/Si, b LSMO/CTO/Si, and c LSMO/STO samples (color online)

(001) oriented and show a high epitaxial quality. The out-of-plane lattice parameters, derived from the θ–2θ diagrams (Fig. 1a–c), are equal to 3.845, 3.900, and 3.805 Å, for LSMO/STO/Si, LSMO/CTO/Si, and LSMO/STO, respectively. We deduce from the small value of the FWHM observed in the θ–2θ recordings and, more specifically, in the rocking scans that the mosaïcity is weak: in the LSMO/CTO/Si sample the FWHM is smaller than 0.1° (e.g., see Fig. 2 which presents the rocking scans related to the [001] lines of LSMO and of CTO) while, in the case of LSMO/STO/Si the spectra are slightly broader with measured FWHM overpassing 0.2°. The full in-plane epitaxy with cubic axes [100] and [010] along the sample edges is demonstrated by the pole figures: typical partial {110} pole ϕ-scans diagrams around $\Psi = 45°$ are shown in Fig. 3 (Ψ is the declination angle between the scattering vector and the direction normal to the film, ϕ is the rotational angle around this direction): all the samples show identical well defined in-plane crystallographic orientations.

Considering the lattice parameter of bulk LSMO (3.876 Å) (Martin et al. 1996), it appears that LSMO/STO/Si and LSMO/STO films are subjected to an in-plane tensile strain while LSMO/CTO/Si is compressed. The in-plane strain $\delta a/a$ can be simply related to the out-of-plane one, $\delta c/c$, through the equation:

$$\frac{\delta a}{a} = -\frac{C_{11}\,\delta c}{2C_{12}\,c} \approx -\frac{1-\nu}{2\nu}\frac{\delta c}{c} \qquad (1)$$

where C_{11} and C_{12} stand for cubic elastic constants and (using an isotropic approximation) ν is the Poisson coefficient. From the published (Rajendran et al. 2003; Bichurin et al. 2003) values of the elastic constants, the in-plane strains $\delta a/a$ can be roughly estimated as $+[0.014; 0.016]$, $+[0.006; 0.007]$ and $-[0.006; 0.007]$, for LSMO/STO, LSMO/STO/Si, and LSMO/CTO/Si, respectively. In the case of LSMO/STO the substrate seems to induce an in-plane clamping of the LSMO film while, for the other samples, the in-plane LSMO lattice depends on the buffer. Anyway, the observed fourfold symmetry around the direction normal to the sample is expected to give rise to a fourfold in-plane magnetic anisotropy showing one of its principal axes parallel to the [110] LSMO crystallographic axis.

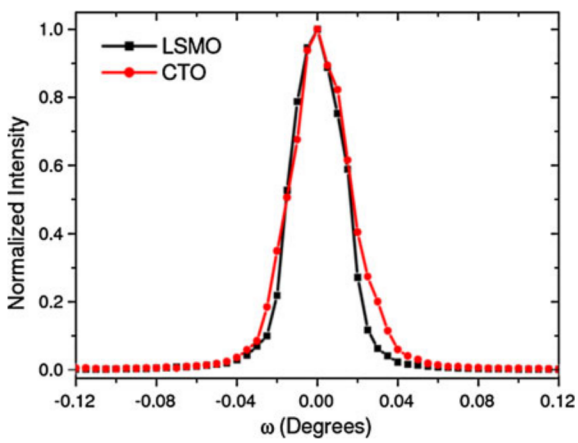

Fig. 2 Rocking curve in ω of the (002) LSMO and CTO lines of the LSMO/CTO/Si sample (color online)

Results and discussion

Static magnetic measurements

The saturation magnetizations were measured using a SQUID up to 400 K under an in-plane applied magnetic field of 5000 Oe (Fig. 4). The values obtained for $4\pi M_s$ at room temperature (294 K) are 2800, 3700, and 4000 Oe for LSMO/STO/Si, LSMO/CTO/Si, and LSMO/STO, respectively. The temperature dependence is approximately described assuming a conventional Brillouin-like behavior with a saturation magnetization lying around 6600 Oe at 0 K. The Curie temperatures (T_c) are 320, 345, and 360 K, respectively. The differences observed for T_c, and, therefore, for $4\pi M_s$ at room temperature (294 K), are probably related to strains variations and to uncontrollable interfacial disorders (Pradhan et al. 2008).

In order to study the magnetic anisotropy at room temperature, the hysteresis loops were measured in all the studied films, using a vibrating sample magnetometer (VSM) with an in-plane applied magnetic field H along various orientations, as shown in Fig. 5 (φ_H is the in-plane angle between H and the [100] axis). The typical behavior is described below through representative LSMO/CTO/Si film. As shown in Fig. 5, differences in shape of the normalized hysteresis loops are observed depending upon the field orientation. For H along [110] ($\varphi_H = 45°$) it consists in a typical easy axis square-shaped loop with a nearly full normalized remanence ($M_r/M_s = 0.95$), a coercive field of about 25 Oe and a saturation field around 70 Oe. As H deviates away from [110], the coercivity decreases and the

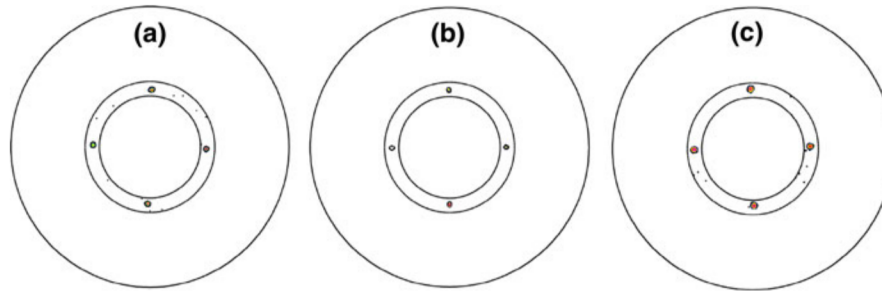

Fig. 3 {110} partial pole figures for the a LSMO/STO/Si, b LSMO/CTO/Si, and c the LSMO/STO samples (color online)

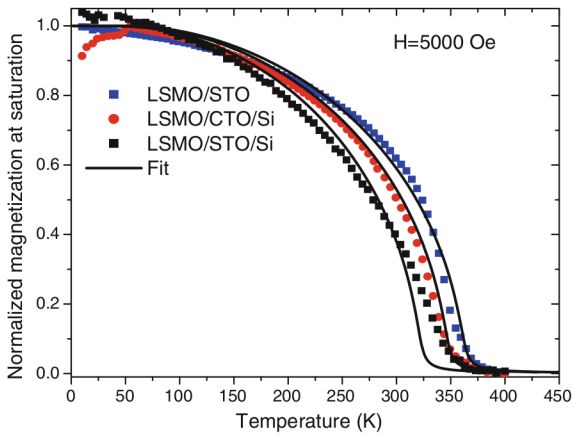

Fig. 4 Temperature dependences of the normalized magnetization $M_s(T)/M_s(0)$ in the three studied LSMO films measured under a 5000 Oe in-plane applied field. The full curves are the calculated variations using a classical Brillouin-like behavior (color online)

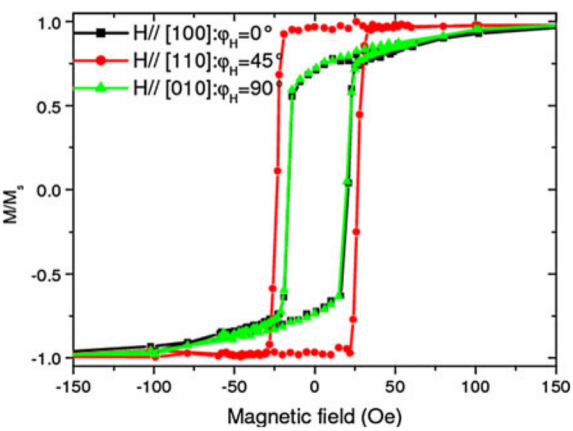

Fig. 5 VSM magnetization loops of the LSMO/CTO/Si sample. The magnetic field is applied parallel to the film surface, at various angles (φ_H) with the [100] axis direction (color online)

hysteresis loop tends to transform into a hard axis loop. The results for $\varphi_H = 90°$ and $\varphi_H = 0°$ are similar: they show a rounded loop with M_r/M_s equal to 0.7 and a saturation field of about 170 Oe. These results qualitatively agree with a description of the in-plane anisotropy in terms of a fourfold contribution with [100] and [010] as hard axes. In addition, the coercive fields of LSMO/STO/Si and LSMO/STO films only slightly differ from each other and are weak compared to the measured one in the LSMO/CTO/Si sample, suggesting that their anisotropy is smaller than in the LSMO/CTO/Si film. As confirmed below by our resonance results the CTO buffer does not affect the above predicted fourfold symmetry of the anisotropy properties but deeply modifies the numerical values of the corresponding parameters. This difference is probably connected to the sign reversal of the in-plane strains but an explanative model is still missing.

Dynamic magnetic properties

The dynamic measurements were carried out using MS-FMR. The MS-FMR setup (Belmeguenai et al. 2009) consists in a home-made mounting which, up to now, only works at room temperature. The resonance frequencies are obtained from a fit assuming a Lorentzian-derivative shape of the recorded data.

As previously published (Belmeguenai et al. 2010), the dynamic properties are tentatively interpreted assuming a magnetic energy density which, in addition to Zeeman, demagnetizing and exchange terms, contains a perpendicular and a fourfold in-plane anisotropy contribution:

$$E = -M_s H[\sin\theta_M \sin\theta_H \cos(\varphi_M - \varphi_H) + \cos\theta_M \cos\theta_H] - \left(2\pi M_s^2 - K_\perp\right)\sin^2\theta_M - \frac{1}{8}K_4(3 + \cos 4(\varphi_M - \varphi_4))\sin^4\theta_M \quad (2)$$

In the above expression, θ_M and φ_M, respectively, represent the out-of-plane and the in-plane (referring

to the [100] axis) angles defining the direction of the magnetization M_s; φ_4 stands for the angle of the fourfold easy axis with [100]. With this definition K_4 is necessarily positive. As done in Belmeguenai et al. (2010), it is often convenient to introduce the effective demagnetization $4\pi M_{\text{eff}} = 4\pi M_s - 2K_\perp/M_s$ and the fourfold in-plane anisotropy field $H_4 = 4K_4/M_s$. (Exchange is not taken into account in Eq. 2 since it does not contribute to the uniform modes studied below.) For an in-plane applied magnetic field H, the studied model provides the following expression of the frequency of the experimentally observable uniform mode:

$$F_r^2 = \left(\frac{\gamma}{2\pi}\right)^2 \left[H\cos(\varphi_M - \varphi_H) + 4\pi M_{\text{eff}} + \frac{K_4}{2M_s}(3 + \cos 4(\varphi_M - \varphi_4))\right] \cdot \left[H\cos(\varphi_M - \varphi_H) + \frac{2K_4}{M_s}\cos 4(\varphi_M - \varphi_4)\right] \quad (3)$$

In the above expression γ is the gyromagnetic factor: $(\gamma/2\pi) = g \times 1.397 \times 10^6$ Hz/Oe.

In the case of an out-of-plane applied magnetic field, high applied fields are needed and, consequently, the fourfold anisotropy contribution can be neglected. It results that the resonance frequency for an out-of-plane applied magnetic field is given by:

$$F_{\text{out}}^2 = \left(\frac{\gamma}{2\pi}\right)^2 [H\cos(\theta_M - \theta_H) - 4\pi M_{\text{eff}}\cos 2\theta_M] \cdot [H\cos(\theta_M - \theta_H) - 4\pi M_{\text{eff}}\cos^2\theta_M] \quad (4)$$

Gyromagnetic g-factor and effective magnetization

The MS-FMR technique, in perpendicular configuration, allows for deriving the values of g and $4\pi M_{\text{eff}}$ from the variation of the resonance frequency versus the magnitude of the perpendicular applied field using Eq. 4 (with $\theta_M = \theta_H = 0$). The typical MS-FMR perpendicular field-dependence of this resonance frequency for the three samples is shown in Fig. 6. Its variation versus the magnetic field is in excellent agreement with the calculated ones using Eq. 4 with $g = 1.92$ and $4\pi M_{\text{eff}} = 4900$, 3700, and 6100 Oe for LSMO/STO/Si, LSMO/CTO/Si, and LSMO/STO, respectively. Taking into account the static magnetization reported above it results that ($H_\perp$) is negative when LSMO lies on STO and

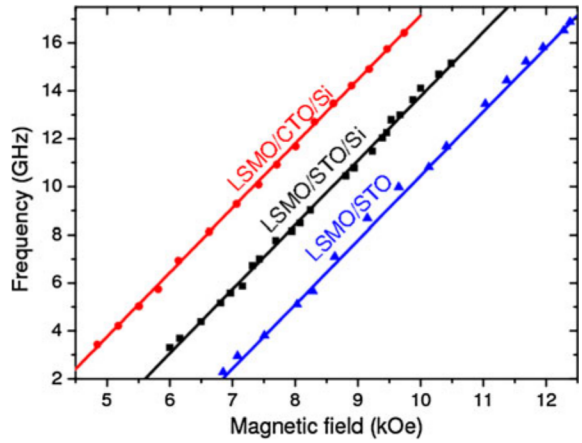

Fig. 6 Field-dependence of the resonance frequency of the uniform excited modes of the three studied samples (LSMO/STO/Si, LSMO/CTO/Si, and LSMO/STO). The magnetic field is applied perpendicular to the film plane. The fits are obtained using Eq. 4 with the parameters indicated in the text and Table 1 (color online)

positive when it lies on CTO (thus implying a perpendicular anisotropy with an anisotropy field $H_\perp = 2\frac{K_\perp}{M_s}$ of about −2500, 200, and −2500 Oe in LSMO/STO/Si, LSMO/CTO/Si, and LSMO/STO, respectively). The observed differences concerning the amplitudes and the sign of the strains in the samples are expected to induce these variations of $H_\perp$. Thus, it appears that this anisotropy field is positive in the case of a compressive strain (LSMO/CTO/Si) and negative in the case of extensive strain (LSMO/STO/Si and LSMO/STO). This change is presumably due to its magnetostrictive origin: the magnetostrictive contribution to the uniaxial anisotropy field derives from the in-plane stress T_{xx} (=T_{yy}) and can be written as:

$$H_{\perp,\text{mstr}} = -2\frac{\lambda_{100}}{M_s}T_{xx} = 2\frac{\lambda_{100}}{M_s}\left(\frac{(C_{11} + C_{12})C_{11}}{2C_{12}} - C_{12}\right)\frac{\delta c}{c} \approx \frac{\lambda\, E\delta c}{M_s\, \nu\, c} \quad (5)$$

In the above equation λ_{100} is the appropriate magnetostrictive coefficient; E is the Young modulus (using the isotropic approximation for which the magnetostrictive coefficient is simply expressed by λ). The reported magnitude of λ (Bichurin et al. 2003) lies around 10^{-5}: it provides a uniaxial anisotropy term corresponding to the kOe range for the observed strains $\delta c/c$ with a sign reversal when the sign of

$\delta c/c$ is changed. Therefore, the main source of this perpendicular anisotropy is most probably the buffer layer dependent strain and can be semi-quantitatively estimated.

Magnetic in-plane anisotropy

MS-FMR allows for dynamic measurements over a large frequency range and, consequently, low external fields can be applied in order to put in evidence small magnetic anisotropies which could not be detected with the high applied magnetic fields used for conventional FMR. Therefore, the in-plane anisotropy terms at room temperature were deduced from the MS-FMR resonance frequency variation versus the direction (defined by φ_H) of a weak in-plane magnetic field. Figure 7a shows typical experimental in-plane angular-dependences of the resonance frequency for the three samples. The anisotropy axes are straightforwardly deduced from the fit of the data with Eq. 3 which implies that the principal anisotropy directions correspond to the extrema of the resonance frequency. The in-plane angular-dependence shows that the samples clearly exhibit a fourfold magnetic anisotropy with an easy axis along [110] ($\varphi_4 = 45°$) (and equivalent directions) while the hard axis lies along [100] (and [010]). These results are in agreement with the predictions derived from the X-rays study in which the pole figures revealed a fourfold symmetry.

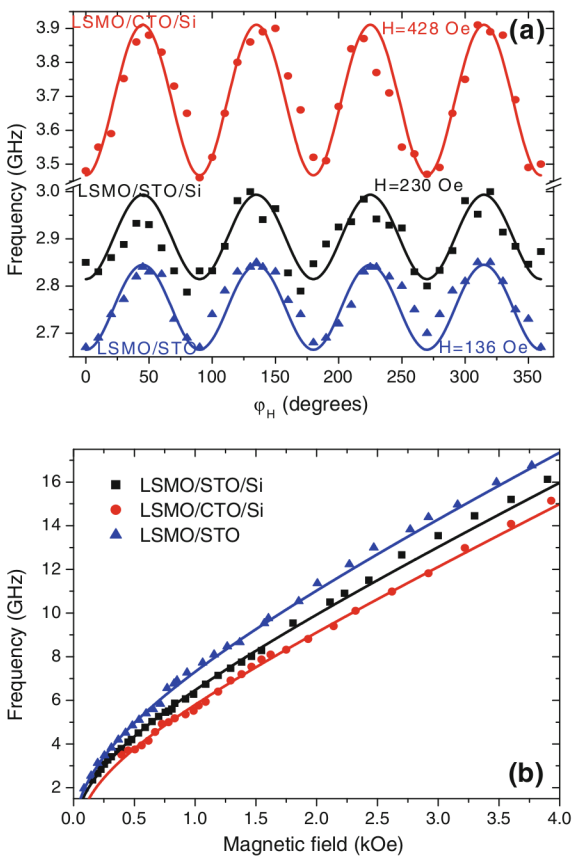

Fig. 7 In-plane a angular-dependence and b field-dependence of the resonance frequency of the uniform mode in the three studied samples. The fits are obtained using Eqs. 3 and 4 with the parameters indicated in the text and in Table 1 (color online)

The values of $H_4 = 4\frac{K_4}{M_s}$ derived from the best fit of our data are found equal to 28, 38, and 100 Oe, respectively, for LSMO/STO/Si, LSMO/STO, and LSMO/CTO/Si.

Finally, the field amplitude dependence of the resonance frequency was studied with H applied in the sample plane. The best fit (assuming that g is unchanged: $g = 1.92$), illustrated in Fig. 7b, is obtained for values of $4\pi M_{\text{eff}}$ significantly different from the derived ones from the measurements with H perpendicular to the film. We find: $4\pi M_{\text{eff}} = 5300$, 3900, and 6500 Oe, to compare to 4900, 3700, and 6100 Oe in LSMO/STO/Si, LSMO/CTO/Si, and LSMO/STO, respectively. These differences may be induced by unavoidable errors in determining the g and $4\pi M_{\text{eff}}$ in the case of a perpendicular applied field arising from a small misalignment between the applied field and the normal to the sample plane. According to our simulations, a misalignment of 1° induces an error of 5% in the determination of g. Finally, the precision

Table 1 Magnetic parameters obtained from the best fits to our experimental results

Sample	LSMO/STO/Si	LSMO/CTO/Si	LSMO/STO
T_c (K)	320	345	360
$4\pi M_s$ (Oe): $T = 0$ K	6700	6700	6600
$4\pi M_s$ (Oe): $T = 294$ K	2800	3700	4000
$4\pi M_{\text{eff}}$ (Oe): $T = 294$ K	5300	3900	6500
$H_\perp = 4K_\perp/M_s$(Oe): $T = 294$ K	−2500	200	−2500
$H_4 = 4K_4/M_s$ (Oe): $T = 294$ K	28	100	38

The values of $4\pi M_{\text{eff}}$ (Oe) are those determined from MS-FMR measurements using an in-plane applied magnetic field

concerning the determination of $4\pi M_{\text{eff}}$ and $H_{\perp}$ remains of a few hundreds of Oersteds. The magnetic parameters of the three samples derived from static and dynamic measurements at 294 K are summarized in Table 1.

Conclusion

The static and dynamic magnetic properties of nearly 50-nm thick LSMO films, deposited on Si substrates overlaid by a 20 nm STO or CTO buffer layers have been studied and compared to a reference LSMO film grown on a STO substrate. Our X-ray diffraction measurements show their excellent epitaxial (001) orientation. Their magnetic behavior is interpreted assuming a magnetic energy density characterized by a strong perpendicular anisotropy and by a weak in-plane anisotropy showing a fourfold symmetry. Both anisotropy values depend on the nature of the buffer layer due to the strain. A good fit of all the experimental data, using appropriate values of the magnetic coefficients describing the free energy, is obtained.

Acknowledgment The authors would like to thank F. Zighem for VSM measurements during this study.

References

Belmeguenai M, Zighem F, Roussigné Y, Chérif SM, Moch P, Westerholt K, Woltersdorf G, Bayreuther G (2009) Microstrip line ferromagnetic resonance and Brillouin light scattering investigations of magnetic properties of Co_2MnGe Heusler thin films. Phys Rev B 79:9–024419

Belmeguenai M, Mercone S, Adamo C, Méchin L, Fur C, Monod P, Moch P, Schlom DG (2010) Temperature dependence of magnetic properties of $La_{0.7}Sr_{0.3}MnO_3$/$SrTiO_3$ thin films on silicon substrates. Phys Rev B 81:054410–054418

Bichurin MT, Petrov VM, Srinivasan G (2003) Theory of low-frequency magnetoelectric coupling in magnetostrictive–piezoelectric bilayers. Phys Rev B 68:0544402–0544413

Bowen M, Bibes M, Barthélémy A, Contour JP, Anane A, Lemaître Y, Fert A (2003) Nearly total spin polarization in $La_{2/3}Sr_{1/3}MnO_3$ from tunneling experiments. Appl Phys Lett 82:233–235

Dediu V, Murgia M, Matacotta FC, Taliani C, Barbanera S (2002) Room temperature spin polarized injection in organic semiconductors. Solid State Commun 122:181–184

Ishii Y, Yamada H, Sato H, Akoh H, Kawasaki M, Tokura Y (2005) Perovskite manganite magnetic tunnel junctions with enhanced coercivity contrast. Appl Phys Lett 87:22509–22509-3

Martin MC, Shirane G, Endoh Y, Hirota K, Moritomo Y, Tokura Y (1996) Magnetism and structural distortion in the $La_{0.7}Sr_{0.3}MnO_3$ metallic ferromagnet. Phys Rev B 53:14285–14290

Park JH, Vescovo E, Kim HJ, Kwon C, Ramesh R, Venkatesan T (1998) Magnetic properties at surface boundary of a half-metallic ferromagnet $La_{0.7}Sr_{0.3}MnO_3$. Phys Rev Lett 81:1953–1956

Pradhan AK, Hunter D, Williams T, Lasley-Hunter B, Bah R, Mustafa H, Rakhimov R, Zhang J, Sellmyer DJ, Carpenter EE, Sahu DR, Huang JL (2008) Magnetic properties of $La_{0.6}Sr_{0.4}MnO_3$ thin films on $SrTiO_3$ and buffered Si substrates with varying thickness. J Appl Phys 103:023914–023918

Rajendran V, Kumaran SM, Sivasubramanian V, Jayakumar T, Raj B (2003) Anomalies in elastic moduli and ultrasonic attenuation near ferromagnetic transition temperature in $La_{0.67}Sr_{0.33}MnO_3$ perovskite. Phys Stat Sol A 195:350–358

Warusawithana MP, Cen C, Sleasman CR, Woicik JC, Li Y, Kourkoutis LF, Klug JA, Li H, Ryan P, Wang LP, Bedzyk M, Muller DA, Chen LQ, Levy J, Schlom DG (2009) A ferroelectric oxide made directly on silicon. Science 324:367–370

Xiong ZH, Wu D, Vardeny ZV, Shi J (2004) Giant magneto-resistance in organic spin valves. Nature 427:821–824